Spectrochimica Acta Part A: Molecular and Biomolecular Spectroscopy 261 (2021) 120007

Contents lists available at ScienceDirect

Spectrochimica Acta Part A: Molecular and Biomolecular Spectroscopy

journal homepage: www.elsevier.com/locate/saa

Analysis of the tautomeric equilibrium of two red monoazo dyes by UV–Visible, Raman and SERS spectroscopies

Giulia Vannucci [a,1], Maria Vega Cañamares [b,*], Silvia Prati [a], Santiago Sanchez-Cortes [b]

[a] Microchemistry and Microscopy Art Diagnostic Laboratory, University of Bologna, Via Guaccimanni 42, 48121 Ravenna, Italy
[b] Instituto de Estructura de la Materia, IEM-CSIC, calle Serano 121, 28006 Madrid, Spain

HIGHLIGHTS

- Acid red 26 and Acid red18 have the OH group in *ortho*- respect to the N=N group.
- UV–Vis, Raman and SERs analysis were performed at different pH conditions.
- The keto tautomer is prevalent at pH < pK_a of the dyes, and the hydro at pH > pK_a.
- Only the keto tautomer of the red azo dyes can be detected by SERS spectroscopy.

GRAPHICAL ABSTRACT

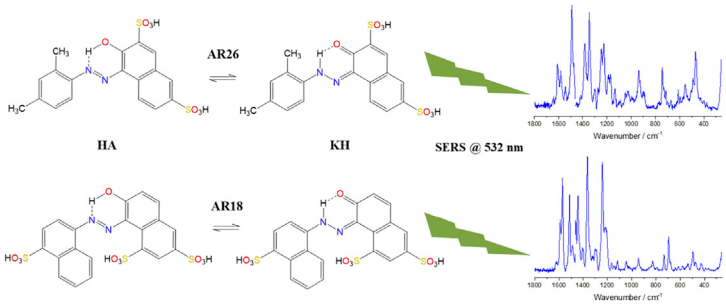

ARTICLE INFO

Article history:
Received 17 March 2021
Received in revised form 20 May 2021
Accepted 22 May 2021
Available online 26 May 2021

Keywords:
AR26
AR18
Raman
DFT calculations
pH

ABSTRACT

Acid Red 26 and Acid Red 18 are two early synthetic dyes belonging to the monazo dye class. The molecular structure of this class of dyes is characterized by the chromophoric azo group (N=N) generally attached to benzene or naphthalene derivatives containing electron withdrawing and/or donating groups as substituents. As both red dyes have an OH group in *ortho*- position respect to the azo group, they undergo an azo-hydrazone tautomerism. In this work, UV–Vis, Raman and SERS spectroscopic analysis of the red dye solutions were carried out at different pH conditions, in order to evaluate the preponderance of one tautomer over the other as a function of the pH. Different experimental conditions were tested in order to find the best ones for the detection of both dyes. Thus, Raman spectra of the powder and aqueous solutions of AR26 and AR18 were obtained at the natural pH of the solutions, and above and below that value. The SERS analysis of the dye solutions were carried out at various pH values between 2 and 10, and with excitation at 442, 532 and 633 nm. The molecular structure and the theoretical Raman spectra of the two tautomers of both red dyes were calculated by DFT methods. The obtained results were used for the assignment of the Acid Red 26 and Acid Red 18 vibrational modes. Finally, a textile sample dyed with AR18 was analyzed by SERS.

1. Introduction

The study of organic coloring materials used in cultural heritage objects provides useful information for dating, authentication, conservation treatments, and art history in general. Synthetic dyes are not as widely studied as natural dyes, since the latter are typically considered of more artistic and historic relevance. However, the study of modern and contemporary art is widely recognized as

* Corresponding author at: Instituto de Estructura de la Materia, IEM-CSIC, Serrano 121, 28006 Madrid, Spain.
E-mail address: mvca@iem.cfmac.csic.es (M.V. Cañamares).
[1] Current address: Rathgen Research Laboratory, National Museums in Berlin, Schloßstraße 1, 12163 Berlin, Germany.

https://doi.org/10.1016/j.saa.2021.120007
1386-1425/

one of the most difficult and pressing challenges in conservation science. Indeed, the ease in production and employment of these materials was responsible for their huge widespread, accompanied by a lack of scientific knowledge and comprehension of adequate conservation treatments [1].

Azo dyes are synthetic organic colorants which have better properties than natural dyes in tinctorial power, range and brilliance of shade, stability and ease of application. The molecular structure of this class of dyes is characterized by the chromophoric azo group (N=N) generally attached to benzene or naphthalene derivatives containing electron withdrawing and/or donating groups as substituents. These aromatic side groups aid in the stabilization of the azo group by extending the delocalized system [2].

Acid Red 26 (AR26, CI 16150) and Acid Red 18 (AR18, CI 16255) are part of the azo dyes class. Both were synthesized by H. Baum in 1878, and are commercially sold as a disodium and trisodium salt powder, respectively. AR26, also known as Ponceau RR, has a bordeaux-red color as a powder, but when solubilized in water, the solution turns to a bright red hue. The structure of AR26 consists of a disulphonated naphtol and a dimethyl benzene ring attached to the azo group. AR26 is used for dying textiles, such as wool, silk and nylon. Actually, it was found in a group of Turkoman rugs, replacing madder, and also mixed with it [1]. Besides, it is used as colorant for inks, paper pigments (heavy metal salts) wood stains, leather, drugs, cosmetics, and food [3]. AR26 is common in biological studies, typically to stain thin sections [4,5]. AR18, also known as Ponceau 4R and Cochineal red A, has a strawberry red color and is stable to light, heat, and acids [6]. Its structure has a sulphonated naphthalene and a disulphonated naphtol attached to the azo group. Similar to AR26, AR18 is employed in the textile manufacture, and for coloring inks, paper, plastics, wood stains, leather, drugs, cosmetics and food [3].

Raman spectroscopy has been proved as an efficient non-destructive technique for identification of inorganic materials in artworks [7,8]. However, the application of this technique in the analysis of organic dyes is limited since the high fluorescence emitted by the organic materials can mask the Raman emission preventing the analysis of these compounds. The use of SERS (Surface-enhanced Raman Scattering) can overcome this problem due to the huge intensification of the Raman emission and the fluorescence quenching that occurs on metal nanostructures [9]. SERS has been successfully used for the detection of trace amounts of organic dyes in works of art [10]. Indeed, a database of the Raman and SERS spectra of a group of acid red dyes, including AR26 and AR18 was published in 2017 [11]. However, acid dyes typically require much of an effort to be investigated, as they get electrostatically repulsed by the net negative charge of the nanoparticles interphase, which prevents the interaction analyte-substrate, as observed in the case of Acid Orange 20 [12]. Thus, Cessaratto *et al.* [11] could only obtain SERS spectra of the acid dyes at a concentration of 10^{-2} M, which is too high for this spectroscopic technique. This was due to the lack of appropriate pH conditions.

Phenylazonaphthols and azonaphthols derivatives, such as AR26 and AR18, respectively, undergo an azo-hydrazone tautomerism [13]. This behavior is common when the OH group is in *ortho*- or *para*- position respect to the azo (N=N) group. The stability of each tautomer is strictly dependent on the ability to form intra- and intermolecular hydrogen bonding. Neutral pH conditions and electron withdrawing substituents, such as SO_3^-, favor the azo tautomer through intramolecular hydrogen bonding, while high pH and electron donating groups favor the hydrazone through intermolecular hydrogen bonding [14]. In contrast to AO20 [12], AR26 and AR18 are subjected to intramolecular hydrogen bonding between the hydroxylic hydrogen and the corresponding azo linkage (Fig. 1).

In the present work, AR26 and AR18 were studied by means of UV–Vis, Raman and SERS spectroscopies, as a continuation of our previous research paper on AO20 [12]. Both red azo dyes have

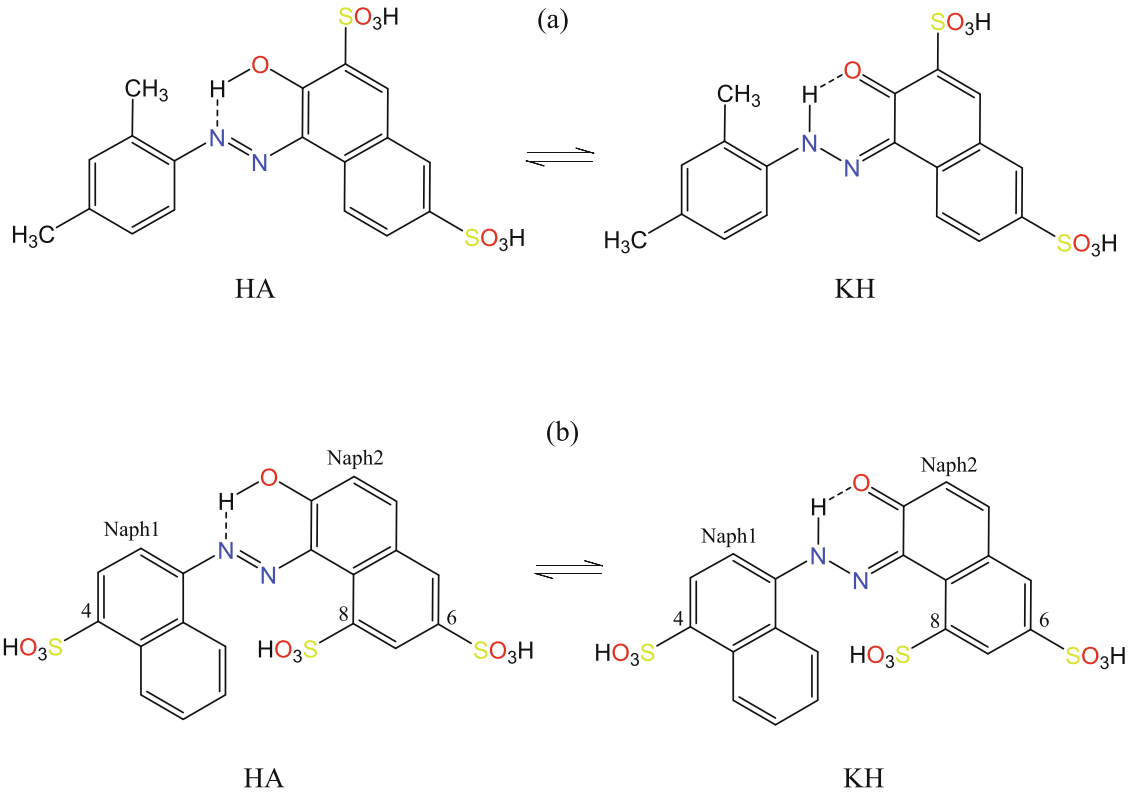

Fig. 1. Molecular structure of the hydro (HA) and keto (KH) tautomers of the (a) AR26 and (b) AR18 dyes.

the hydroxyl group in *ortho-* position, differently to the orange one, which has it in *para-*. Thus, a different behavior related to the acid-base tautomeric equilibrium is expected from that of AO20. The spectroscopic analysis of the red dye solutions was carried out at different pH conditions, in order to evaluate the preponderance of one tautomer over the other as a function of the pH. Different experimental conditions were tested in order to find the best ones for the detection of both red mozoazo dyes. Theoretical DFT calculation of the two tautomers were also performed and used as an aid for the vibrational analysis.

2. Materials and methods

2.1. Reagents

$AgNO_3$, hydroxylamine, trisodium citrate dihydrate and sodium hydroxide were purchased from Sigma-Aldrich. Nitric acid was purchased from Merck. AR26 and AR18 were purchased from Tokyo Chemical Industry (TCI) as sodium salts. All aqueous solutions used for the silver colloid synthesis were prepared using MilliQ water.

The AR18 dyed fibers were provided to the Microchemistry and Microscopy Art Diagnostic Laboratory (M2ADL) of Ravenna by the Rijksdienst voor het Cultureel Erfgoed institution (Amsterdam) in the contest of CHARISMA project. These samples are part of a selection of historically documented synthetic dyes, relative to the period 1856–1900.

2.2. Preparation of Ag nanostars

The nanostars colloid was prepared following the procedure reported by García-Leis *et al.* [15]. Such SERS substrate is prepared by a two-steps reduction process of $AgNO_3$, first with neutral hydroxylamine, and the second with trisodium citrate dihydrate. UV–Vis spectra of the prepared Ag NST were registered in order to analyze the surface plasmon resonance of the Ag suspensions. One hour after the synthesis, Ag NST showed a maximum absorption at 386 and 407 nm, assigned to quadrupoles and surface plasmon resonances (SPR), respectively. The intensity of the absorption at wavelengths higher than 500 nm is due to the heterogeneous nature of the Ag NST [15], which has the advantage of being able to enhance the signal of compounds characterized by maxima of absorbance occurring over a wide range in the spectrum. This "tail" is kept for the different pH tested (Fig. S1a). The intensity of the extinction maximum decreases for acidic pH (while this band increases again for basic pH): this behavior can be attributed to the hydroxylamine employed in the synthesis of the colloid, which results to be sensitive and not stable at acidic pH. The UV–Vis spectra of the Ag NST after 18 h (Fig. S1b), show very little differences with the spectra after 1 h. There is a slight decrease of the maximum at 386 nm, due to the quadrupoles, and a slight increase of the band at 413 nm, assigned to SPR. After 18 h, also the pH of the solution changed (from 5.5 to 5–5.3).

2.3. Preparation of samples

For the UV–Vis and Raman analysis, stock solutions of the dyes were prepared at a concentration of 10^{-2} M. Solutions at different pH values were obtained by the addition of suitable micro-volumes of diluted HNO_3 or NAOH.

For the SERS analysis, 10^{-4} M aqueous solutions of AR26 and AR18 were prepared. Then, an aliquot of 100 μL was taken and added to 900 μL of the nanostars colloid, reaching a concentration of 10^{-5} M.

For the SERS analysis of the AR18 dyed fibers a previous extraction process was carried out. A small piece of the wool thread was cut, and the fibers were put inside a vial with MilliQ water and heated for one hour. After that time, a light red solution was obtained. Part of this solution was put on a glass slide followed by the addition of 5 μL of 2x concentrated Ag NST and 0.8 μL of HNO_3 0.2 M. A coverslip was put on top and the mixture was analyzed under the microscope at 532 nm. The pH of the mixture was ~2.

2.4. Instrumentation

The UV/VIS/NIR absorbance spectra of the dyes solutions and of the colloidal dispersions were obtained with a Shimadzu 3600 UV/VIS/NIR spectrometer equipped with ^2H and W lamps, a photomultiplier (UV/VIS), and a InGaAs and a PbS (NIR) detectors. The baseline reference sample was prepared with 3 mL of MilliQ water.

Raman and SERS spectra at 442 and 532 nm were collected with a Renishaw inVia Raman Spectrometer, equipped with a Leica microscope, and an electrically refrigerated CCD camera. He:Cd and Nd:YAG lasers were used as 442 and 532 nm excitation lines, respectively. Measurements were taken using a Rayleigh line filter, and different gratings were coupled with the different laser sources: 1800 l/mm and 2400 l/mm for the 532 and 442 nm lines, respectively. Spectra were collected in the range 2000–100 cm^{-1}. The maximum power at the samples when exciting at 442 and 532 nm were 3 and 5 mW, respectively. Spectra were registered with an integration time of 10 s.

Raman and SERS spectra at 633 and 785 nm were collected with a Renishaw RM2000 Raman Microscope System equipped with a Leica microscope and an electrically refrigerated charge-coupled device camera (CCD). He—Ne and diode lasers were used as 633 and 785 nm excitation lines, respectively. Spectra were collected in the range 1800–100 cm^{-1}. The maximum power at the samples with the 633 and 785 nm lasers were 2.5 and 2 mW, respectively. Spectra were registered with an integration time of 10 s.

2.5. DFT calculations

For the hydro (HA) and keto (KH) tautomers of AR26 and AR18, the optimization of the ground state of the singlet structures and the calculation of the theoretical Raman spectra were performed with DFT using the Gaussian 09 package [16]. Calculations were carried out considering ionized the sulfonate groups, as in the experimental conditions used in this work these groups are deprotonated. All calculations were performed in vacuum conditions, using a B3LYP hybrid exchange correlation functional in combination with 6-31G** as a basis set. Upon optimization of the molecular geometry, Raman spectra were obtained. No imaginary wavenumbers were observed in the calculated spectra. GaussView 5.09 was employed to view data and output images. Detailed assignments of the vibrational normal modes were based on the best fit comparison of the wavenumbers of calculated and experimental Raman bands. A scaling factor of 0.9627 was employed in this work, as these factors are commonly used in the calculated spectra in order to correct the correlation effects that are only partially accounted for in DFT [17].

3. Results and discussion

3.1. UV–Vis spectra of aqueous solutions at different pH

Fig. 2a and b show the UV–Vis absorption spectra at different pH values of AR26 and AR18, respectively.

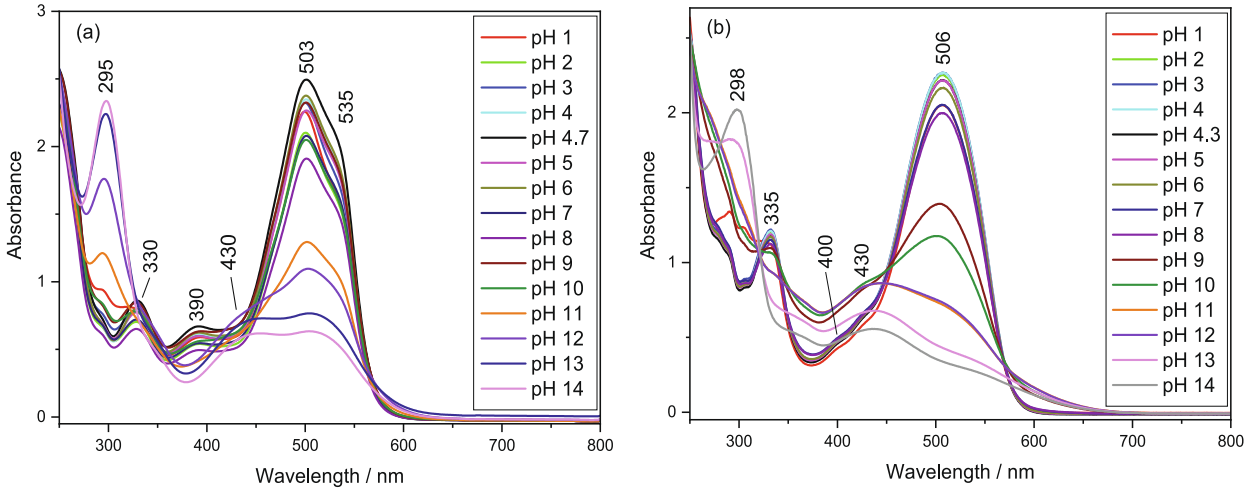

Fig. 2. UV–Vis spectra of 10^{-4} M (a) AR26 and (b) AR18 aqueous solutions at different pH values.

For these types of dyes, the KH tautomer is bathocromic shifted compared to the HA, and has usually a higher tinctorial strength [18]. Therefore, the band of AR26 at higher wavelength (535 nm) corresponds to the KH tautomer, while the band at 503 nm corresponds to the HA. For pH $\leq$ 10, AR26 also shows absorptions at 330 ($\pi \rightarrow \pi^*$ of the naphtalene moiety with partly lost aromaticity in KH) and 390 nm (non-permitted n $\rightarrow$ π^* of the C═N). For pH $\geq$ 11 the absorption at 295 nm increases drastically ($\pi \rightarrow \pi^*$ electronic transition of the naphtalene moiety with restored aromaticity), while the bands at 330 and 390 nm disappear, both linked to KH. At the same time, a new band at 430 nm is observed, which is ascribable to the n $\rightarrow$ π^* electronic transition of the chromophore system in the HA deprotonated tautomer, similarly to what was observed for AO20 [12]. Moreover, the band at 535 nm, attributed to the KH tautomer, disappears. As can be evicted, the two AR26 tautomers exist in equilibrium until pH 11, being KH the prevalent one. Due to the presence of the hydroxyl group in *ortho-* position, the HA tautomer is not deprotonized until pH 11–12 (pK_a (OH) = 11.59) [19], where changes start to occur, and the prevalent tautomer becomes the deprotonated azo one (HA^-).

The AR18 aqueous solution (10^{-4} M) had a pH in the range ~4–4.4. At pH lower than 9, the spectra (Fig. 2b) are characterized by a maximum at 506 nm ascribable to the $\pi \rightarrow \pi^*$ electronic transition of the chromophore system in the KH tautomer. A second band at around 335 nm is also present ($\pi \rightarrow \pi^*$ of the naphtalene moiety with partly lost aromaticity due to the KH formation), together with two broad but non-intense absorptions at around 400 (n $\rightarrow$ π^* of C═N) and 430 nm (n $\rightarrow$ π^* of N═N) [20]. The absorption profile characterizing the UV–Vis spectra at pH 1–8 range starts to be modified at pH 9, where a decrease of the λ_{max} in the visible range, the increase of the shoulder at 430 nm and 290–300 nm, and the decrease of the absorption at around 330 nm are observed. Similar to AR26, the modification in the UV–Vis absorptions can be attributed to the preponderance of the KH tautomer (always in equilibrium with the HA) until a pH around 9. Overcoming this pH value, the OH of AR18 HA starts to be deprotonized (pK_a (OH) = 11.5) [21], and the equilibrium shifts towards HA^-, hence the bands characteristic of KH decrease in intensity. The pK_a values for the other acidic groups in AR18 are: −0.6 (8-SO_3H), 0.4 (6-SO_3H), 0.9 (4-SO_3H) and 2.7 (—N═N—) [21]. Therefore, all the sulfonated groups are deprotonated in the aqueous solutions used in this work.

The comparison of the UV–Vis absorption spectra of AR26 and AR18 with that of AO20, previously studied [12], shows some differences that are related to the stability of each tautomer. This fact is explained by a factor that mostly influence the stability of a tautomer over the other, the position of the hydroxyl group in the naphtalene moiety. In AO20 it is found in *para-* position in respect to the chromophore (N═N), therefore, the KH is stable in a reduced pH range (until 4.7). This is due to the structural impossibility of the hydroxyl hydrogen atom to participate in a hydrogen bond that leads to the six-membered ring formation. Therefore, a pH above 4.7 favors the deprotonated HA tautomer. However, the presence of the hydroxyl group in *ortho-* thermodynamically stabilizes the KH tautomer in AR26 and AR18 for a more extended pH range, up to pH 11 and 9, respectively. The exceeding of this pH values causes the OH to deprotonate, favoring the HA^- tautomer.

Moreover, AR26 and AR18 also show differences: in AR26 the HA tautomer seems to be present in a higher amount in respect to AR18. It is believed [22] that when an electron-withdrawing group as SO_3^- is found in the aromatic ring containing the OH, and an electron donor group as CH_3 is found in the opposite ring, the HA tautomer may be found in a higher amount than expected (and vice versa).

3.2. Raman spectra of aqueous solutions at different pH and DFT calculations

Raman spectra of AR26 and AR18 in aqueous solutions at different wavelengths are presented in Fig. S2. The most intense spectra were obtained at 633 nm, even though both dyes show pre-resonant conditions at 442 and 532 nm. Furthermore, for this reason, Raman spectra at those wavelengths could not be obtained at the full power, giving rise to much less intensity. Thus, the pH study of the dye solutions at different pH values was carried out at 633 nm.

3.2.1. AR26

Fig. 3a shows the Raman spectra at 633 nm of 10^{-2} M AR26 solutions at different pH together with the DFT calculated spectra of the two ionized KH and HA tautomers. The obtained geometries show a planar structure on both ionized species (Fig. S3a).

The DFT calculated Raman spectra of KH and HA show a good fit with the experimental Raman spectra of each tautomer, not only in the wavenumbers but also in the intensity of the bands. This indicates the suitability of the level of theory used and an appropriate selection of basis set for the AR26 tautomers. The assignments of vibrational normal modes derived from the calculations for the KH and HA ionic species are shown in Table 1.

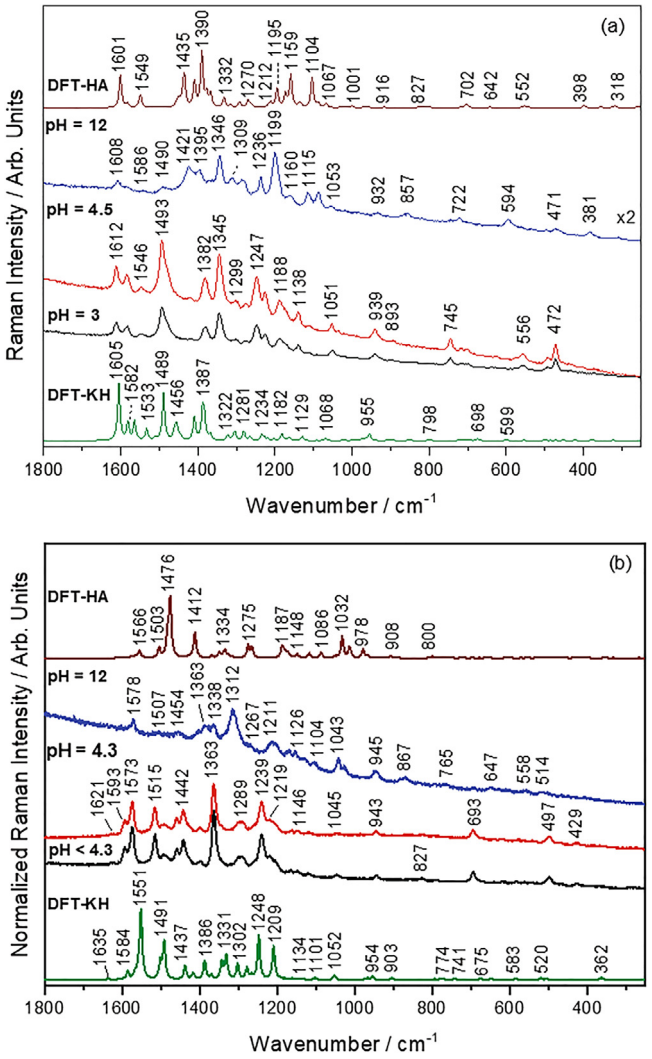

Fig. 3. DFT calculated Raman spectra of the KH and HA tautomers, and experimental Raman spectra at 633 nm of 10^{-2} M aqueous solutions at different pH values of (a) AR26 and (b) AR18.

The Raman spectra of AR26 aqueous solutions at pH 3, pH 4.5 and those with a pH between 4.5 and 9 (not shown), do not show any differences, indicating that the same molecular structure is prevalent in this wide pH range (3–9). The main Raman bands of these spectra are shown at 1612, 1585, 1546, 1493, 1382, 1345, 1299, 1273, 1247, 1226, 1188, 1172, 1138, 1051, 930, 745, 718, 702, 556, 492 and 472 cm^{-1}. Specifically, the appearance of the bands at 1585, 1546, 1372, 1273, 1226, 1188 and 1172 cm^{-1}, that include vibrations of functional groups of the KH tautomer, such as ν(C═O), $\nu(C{=}C)_{conj}$, δ(NH) and ν(N—N), confirms the presence of this tautomer. This was also corroborated by the results obtained by UV–Vis spectroscopy. KH is the tautomer present at acid pH.

At pH above pH 10 (Fig. S4a), several differences are observed in the Raman spectra, showing the co-existence of the two tautomers. Moreover, the spectrum at pH 12 (Fig. 3a) show lower intensity and S/N ratio than the spectra at acidic pH. The most important bands of this spectrum are observed at 1608, 1490, 1421, 1395, 1346, 1309, 1281, 1236, 1199, 1160, 1115, 1087, 1053, 932, 857, 722, 594, 471 and 381 cm^{-1}. Raman bands at 1586, 1490, 1421, 1395, 1346, 1309, 1236, 1199, 1160, 1115, 1053 and 744 cm^{-1} are assigned to δ(OH) ν(N═N), ν(C—O) and γ(OH), which are characteristics of HA. Thus, both UV–Vis and Raman spectra indicate that this tautomer is present at pH 12.

When the pH increases from 9 to 12 the Raman bands associated with the KH tautomer decrease and those related to HA increase. This fact shows that the tautomeric equilibrium is shifted to HA as the pH increases above 9.

It is important to note that the Raman spectra at acidic and alkaline pH share more similarities when compared to those of the structurally related dye AO20 [12] Thus, it can be deduced that an equilibrium between both AR26 tautomers exists in a wider pH range (up to pH 10), where KH is the prevalent one. However, the bands assigned to that tautomer does not completely disappear at pH ≥ 10, but highly decrease in intensity. This support the fact that as an equilibrium takes place between the two tautomers a certain quantity of the second less-favoured tautomer is always found.

As mentioned above, the pK_a of the OH group in HA is 11.59 [19]. Therefore, Raman spectra of HA at pH 12 would correspond to the deprotonated tautomer. Thus, the differences between the Raman spectra at pH 10 and 12, such as the decrease of the bands at 1586, 1490 and 1245 cm^{-1}, assigned to δ(OH), can be attributed to the deprotonation of the OH group. This process leads to the delocalization of the electronic charge throughout the molecular structure of HA^-.

As explained before, in AO20 the spectral modifications occur for pH > 4.7, at much lower pH compared to AR26, due to the different positions of the hydroxyl group in the two molecules. The OH group in AO20 is in *para-* position related to the N═N group, in contrast to AR26, with found in *ortho-*. In the first case, the formation of a six-membered ring by means of a hydrogen bond between OH and N═N is prevented. Thus, the hydroxyl group is available for deprotonation, shifting the tautomeric equilibrium to HA at a lower pH (4.7). In the second case (AR26), the closer position of the OH and N═N groups make possible the interaction by hydrogen bond leading to the formation of a six-membered ring. As this ring is highly stable, the deprotonation of the OH, and the subsequently formation of the HA tautomer occurs at much higher pH conditions (9).

3.2.2. AR18

The Raman spectra at 633 nm of AR18 aqueous solutions in different pH conditions together with the DFT calculated spectra of KH and HA are shown in Fig. 3b. The optimized structures of the tautomers with the three sulphonate groups deprotonated are shown in Fig. S3b. It is interesting to note that none of these geometries are planar. This can be explained by the steric hindrance produced by the proximity between naphthalene 1 ring and the SO_3^- group in position 8 in naphthalene 2. This makes both aromatic moieties to be in different planes with a C—N—N—C angle of around 174°. According to Almeida *el at.* [23], the value of this torsion angle is due to the strong hydrogen bond between N═N/N—H and O—H/O═C, which is the responsible of maintaining the N═N group almost in plane. However, the geometry of the ionized tautomers of AR26 is planar and strong hydrogen bonds are formed as well. Thus, the non-planarity observed in the case of AR18 should be attributed to the presence of the bulky SO_3^- group in position 8.

The Raman spectra of AR18 aqueous solutions at acid pH (Fig. 3b) show bands at 1593, 1573, 1515, 1491, 1458, 1442, 1398, 1363, 1296, 1289, 1239, 1219, 1164, 1146, 1119, 1045, 943, 693, 497 and 426 cm^{-1}. No differences are observed in the spectral profile of the dye at the pH at which the solution remains after direct solubilization (pH = 4.5) or after acidification (pH < 4.5). The assignment of the experimental Raman bands is displayed in Table 2. According to this assignment, AR18 exists as the KH tautomer at acidic pH. Thus, the band at 1593 cm^{-1} is associated to $\nu(C{=}C)_{conj}$ and ν(C═O), the one at 1573 cm^{-1} to ν(N—N) and δ(NH), that at 1515 cm^{-1} to δ(NH), those at 1442 and 1239 cm^{-1} to ν(N—N), and that at 1289 cm^{-1} to ν(N—N) and ν(C═O). As in

Table 1
Main experimental and calculated Raman wavenumbers (cm^{-1}) of AR26 aqueous solutions at different pH, and assignments derived from the DFT calculations (B3LYP/6-31G**).

ν_{exp} (cm^{-1})[a] AR26 pH = 3	ν_{exp} (cm^{-1})[a] AR26 pH = 4.5	ν_{exp} (cm^{-1})[a] AR26 pH = 12	ν_{calc} (cm^{-1}) AR26 scaled	AR26 tautomer	Band assignment[b]
1612 *m*	1612 *m*		1605	KH	$\nu(CC)_{benz}$
		1608 *m*	1601	HA	$\nu(CC)_{benz}$
1585 *m*	1585 *m*		1582	KH	$\nu(CC)_{naph}$, $\nu(C{=}C)_{conj}$, $\delta(NH)$
		1586 *vw*	1582	HA	$\nu(CC)_{naph}$, $\delta(OH)$
1546 *w*	1546 *w*		1533	KH	$\nu(CC)_{naph}$, $\delta(NH)$, $\nu(C{=}C)_{conj}$, $\nu(CN)$
		1543 *vw*	1549	HA	$\nu(CC)_{benz}$, $\delta(CH_3)$
1493 *vs*	1493 *vs*		1489	KH	$\nu(CC)_{benz}$, $\delta(CH_3)$, $\nu(CN)$
		1490 *w*	1496	HA	$\nu(CC)_{naph}$, $\delta(OH)$
		1421 *m*	1435	HA	$\nu(N{=}N)$, $\delta(CH_3)$, $\nu(C{-}O)$, $\nu(CC)$
1419 *vw*	1419 *vw*		1409	KH	$\nu(CC)_{benz}$, $\nu(CN)$, $\delta(CH_3)$
		1395 *m*	1408	HA	$\nu(N{=}N)$, $\delta(OH)$, $\nu(CC)_{naph}$
1382 *m*	1382 *m*		1387	KH	$\nu(CC)_{benz}$, $\nu(CN)$, $\delta(CH_3)$, $\nu(C{=}O)$
1345 *s*	1345 *s*		1368	KH	$\delta(CH_3)$
		1346 *s*	1332	HA	$\nu(CC)_{benz}$, $\delta(OH)$
		1309 *m*	1315	HA	$\nu(CC)_{naph}$, $\delta(OH)$
1299 *w*	1299 *w*		1304	KH	$\nu(CC)_{benz}$, $\delta(CH_3)$
		1281 *m*	1292	HA	$\nu(CC)_{benz}$, $\delta(CH_3)$
1273 *w*	1273 *w*		1281	KH	$\nu(N{-}N)$, $\delta(CH)$, $\nu(CC)_{naph}$
1248 *s*	1248 *s*		1265	KH	$\delta(CH)$, $\delta(CNN)$, $\delta(CH_3)$
		1236 *m*	1212	HA	$\delta(CCC)_{benz}$, $\delta(CH)$, $\nu(C{-}CH_3)$, $\delta(OH)$
1226 *m*	1226 *m*		1228	KH	$\nu(N{-}N)$, $\delta(CH)$, $\delta(CH_3)$
		1199 *vs*	1195	HA	$\delta(CH)$, $\delta(OH)$, $\nu(CN)$
1188 *m*	1188 *m*		1182	KH	$\delta(CH)$, $\nu(N{-}N)$
1172 *vw*	1172 *vw*		1164	KH	$\nu(S{=}O)$, $\delta(CH)$, $\nu(N{-}N)$
		1160 *w*	1172	HA	$\nu(S{=}O)$, $\delta(CH)$, $\delta(OH)$
1138 *w*	1138 *w*		1129	KH	$\delta(CH)$
		1115 *m*	1104	HA	$\delta(CH)$, $\nu(CN)$, $\delta(OH)$, $\rho(CH_3)$
1111 *vw*	1111 *vw*		1092	KH	$\delta(CH)$, $\delta(CNN)$, $\rho(CH_3)$
		1087 *m*	1087	HA	$\delta(CH)$, $\delta(CNN)$
		1053 *w*	1067	HA	$\delta(CH)$, $\delta(OH)$
1051 *w*	1051 *w*		1068	KH	$\delta(CH)$, $\nu(CS)$
939 *w*	939 *w*		955	KH	$\nu(S{=}O)$, $\delta(CH)$, $\delta(CNN)$
		932 *w*	916	HA	$\gamma(CH)$, $\delta(CCC)_{benz}$, $\nu(C{-}CH_3)$
893 *vw*	893 *vw*		851	KH	$\delta(CNN)$, $\delta(CCC)$
		857 *w*	827	HA	$\gamma(CH)$, $\delta(CCC)_{naph}$, $\delta(CNN)$
745 *w*	745 *w*		721	KH	$\delta(CCC)$
		744 *w*	719	HA	$\gamma(OH)$, $\delta(CCC)_{naph}$, $\gamma(CCC)_{benz}$
		722 *w*	702	HA	$\delta(CCC)$
716 *vw*	716 *vw*		698	KH	$\gamma(CCC)_{benz}$, $\nu(C{-}CH_3)$
700 *vw*	700 *vw*		673	KH	$\delta(CCC)_{naph}$, $\delta(SO_3)$, $\nu(C{-}CH_3)$
		594 *m*	584	HA	$\delta(CCC)_{benz}$, $\gamma(CCC)_{naph}$, $\gamma(CNNC)$
556 *w*	556 *w*		552	KH	Skeletal vibrations
		495 *vw*	488	HA	
492 *w*	492 *w*		500	KH	
472 *m*	472 *m*		452	KH	
		471 *w*	449	HA	
		381 *w*	354	HA	

[a] *vw*, very weak; *w*, weak; *m*, medium; *s*, strong; *vs*, very strong; *sh*, shoulder.
[b] ν, stretching; δ, in-plane bending; γ, out-of-plane bending; ρ, rocking.

the case of AR26, a good fit was obtained of the DFT calculated Raman spectra with the experimental ones in both wavenumbers and intensities.

The Raman spectrum at alkaline conditions show lower intensity and S/N ratio than the spectra at acid pH. The main Raman bands are observed at 1571, 1385, 1363, 1312, 1267, 1211, 1152, 1126, 1104, 1043, 1027, 945, 867 and 558 cm^{-1}. These bands indicate the prevalence of HA tautomer at alkaline conditions. In fact, some of these bands are assigned to normal modes of the characteristic functional groups of the HA tautomer, such as ν(N=N) and δ(OH). This is in agreement with the UV–Vis spectra.

Raman bands assigned to the KH tautomer are still observed up to pH 10 (Fig. S4b), although some due to HA, such as those at 1312, 1027, 945 and 514 cm^{-1}, start to be noticed at pH 9. This supports the idea of the equilibrium of KH and HA tautomers and the prevalence of the first one in a wide pH range, as observed for AR26. AR18 has the OH in *ortho*- position from the azo group as well. Thus, the N=N/N-H and the O-H/C=O groups also form a strong hydrogen bond which stabilize the KH tautomer up to highly alkaline pH values. However, at pH 12, AR18 is already deprotonated, as the pK_a value of the OH is 11.5 [21], shifting the tautomeric equilibrium to HA.

3.3. SERS spectra at different pH

No SERS spectra of the AR26 and AR18 10^{-5} M aqueous solutions could be obtained at 633 and 785 nm at any pH conditions. However, at 442 and 532 nm it was possible to obtain SERS spectra due to the existence of pre-resonance conditions for the two tautomers of both dyes, as observed in the UV–Vis spectra (Fig. 2).

It is important to note that good SERS spectra were obtained at 10^{-5} M, unlike Cessaratto *et al.* [11], when the pH of the mixture was conveniently reduced. This effect is attributed to the protonation of citrate ions adsorbed on the surface [12]. In general, these citrate residue ions confer a negative charge to the interfacial surface, preventing the adsorption of anionic molecules, such as AR26 and AR18 dyes, onto the SERS substrate. However, when the citrate

Table 2
Main experimental and calculated Raman wavenumbers (cm^{-1}) of AR18 aqueous solutions at different pH, and assignments derived from the DFT calculations (B3LYP/6-31G**).

ν_{exp} (cm^{-1})[a] AR18 pH < 4.5	ν_{exp} (cm^{-1})[a] AR18 pH = 4.5	ν_{exp} (cm^{-1})[a] AR18 pH = 12	ν_{cal} (cm^{-1}) AR18 scaled	AR18 tautomer	Band assignment[b]
1621 *vw*	1621 *vw*		1635	KH	$\nu(C{=}C)_{conj}$, $\nu(C{=}O)$, $\nu(CN)$, $\delta(NH)$
1593 *m*	1593 *m*		1584	KH	$\nu(C{=}C)_{conj}$, $\nu(C{-}N)$, $\nu(C{=}O)$, $\nu(CC)_{naph2}$
1573 *s*	1573 *s*		1551	KH	$\nu(CC)_{naph1}$, $\nu(N{-}N)$, $\delta(NH)$
		1571 *m*	1556	HA	$\nu(CC)_{naph1}$, $\nu(N{=}N)$, $\delta(OH)$
1515 *s*	1515 *s*		1501	KH	$\nu(CC)$, $\delta(NH)$
		1507 *vw*	1503	HA	$\nu(N{=}N)$, $\nu(CC)_{naph1}$
1491 *w*	1491 *w*		1491	KH	$\nu(C{=}O)$, $\nu(CC)_{naph}$, $\delta(NH)$, $\nu(C{-}N)$
1458 *m*	1458 *m*		1437	KH	$\nu(CC)_{naph1}$
		1454 *vw*, *b*	1427	HA	$\nu(CC)_{naph1}$
1442 *s*	1442 *s*		1417	KH	$\nu(CC)_{naph}$, $\nu(N{-}N)$
		1404 *vw*	1412	HA	$\nu(CC)_{naph1}$, $\delta(OH)$, $\nu(N{=}N)$
1398 *w*	1398 *w*		1386	KH	$\nu(CC)_{naph2}$, $\nu(CN)$
		1385 *m*	1368	HA	$\nu(CC)_{naph2}$, $\delta(OH)$
1363 *vs*	1363 *vs*		1369	KH	$\nu(CC)_{naph1}$, $\nu(CN)$
		1363 *m*	1349	HA	$\nu(CC)_{naph1}$
		1335 *w*	1334	HA	$\nu(CC)_{naph1}$
		1312 *vs*	1315	HA	$\nu(CC)_{naph2}$, $\delta(OH)$
1296 *sh*	1296 *sh*		1302	KH	$\nu(CC)_{naph2}$, $\nu(N{-}N)$, $\delta(NH)$
1289 *m*	1289 *m*		1277	KH	$\nu(N{-}N)$, $\nu(CC)_{naph}$, $\nu(C{=}O)$
		1267 *w*	1265	HA	$\delta(CH)$, $\delta(OH)$
1239 *s*	1239 *s*		1248	KH	$\nu(N{-}N)$, $\nu(C{-}C)$, $\delta(CH)$
1219 *m*	1219 *m*		1209	KH	$\nu(CN)$, $\delta(CH)$, $\nu(C{-}C)$
		1211 *m*	1187	HA	$\delta(OH)$, $\nu(CN)$, $\delta(CH)$
1207 sh	1207 sh		1193	KH	$\nu(CC)_{naph2}$, $\delta(CH)$
		1198 sh	1181	HA	$\delta(CH)$
		1168 *w*	1172	HA	$\delta(OH)$, $\delta(CH)$, $\nu(S{=}O)$
		1152 *w*	1148	HA	$\delta(CH)$, $\nu(S{=}O)$
1146 *vw*	1146 *vw*		1134	KH	$\delta(CH)$, $\nu(S{=}O)$
		1126 *vw*	1117	HA	$\delta(CH)$
1119 *vw*	1119 *vw*		1101	KH	$\delta(CH)$, $\delta(CCC)_{naph2}$
		1104 *w*	1086	HA	$\delta(CH)$, $\nu(CN)$
1045 *w*	1045 *vw*		1052	KH	$\delta(CCC)_{naph1}$, $\delta(CNN)$
		1043 *m*	1032	HA	$\delta(CCC)_{naph1}$, $\delta(CNN)$
		1027 *m*	1013	HA	$\delta(CCC)_{naph1}$, $\delta(CNN)$
		945 *m*	954	HA	$\delta(CCC)_{naph1}$,$\nu(S{=}O)$, $\gamma(CH)$, $\delta(CNN)$
943 *w*	943 *w*		903	KH	$\delta(CCC)_{naph2}$,$\nu(S{=}O)$
		883 *w*	848	HA	$\gamma(CH)$
		867 *w*	800	HA	$\gamma(CH)$, $\delta(CNN)$
827 *vw*	827 *vw*		774	KH	$\delta(CCC)$, $\delta(CNN)$
		765 *vw*	722	HA	$\delta(CCC)_{naph1}$, $\gamma(CCC)_{naph2}$, $\gamma(OH)$
693 *m*	693 *m*		675	KH	$\delta(CCC)$
		692 *vw*	677	HA	$\gamma(OH)$, $\delta(CCC)$
		647 *vw*	601	HA	$\delta(CCC)_{naph1}$, $\gamma(CCC)_{naph2}$, $\delta(SO_3)$
618 *vw*	618 *vw*		583	KH	$\delta(CCC)_{naph1,}$ $\delta(SO_3)$
		558 *vw*	526	HA	Skeletal vibrations
497 *w*	497 *m*		505	KH	
426 *vw*	429 *vw*		414	KH	

[a] *vw*, very weak; *w*, weak; *m*, medium; *s*, strong; *vs*, very strong; *sh*, shoulder.
[b] ν, stretching; δ, in-plane bending; γ, out-of-plane bending.

anions are protonated, the zeta electric potential of this surface decreases favoring the adsorption of these anionic molecules.

3.3.1. AR26

Fig. 4 shows the SERS spectra of AR26 aqueous solutions on Ag NST obtained at different pH conditions. The spectra at 442 nm (Fig. 4a) show a strong background due to the burning of the dye that leads to the appearance of the amorphous carbon broad bands at 1600 and 1400 cm^{-1}. This is due to the high energy of this laser line. The SERS spectra show a strong dependence with the pH. It is necessary to lower the pH until 3 and 2 in order to obtain quite good SERS spectra. At these conditions, intense SERS bands were obtained at 1608, 1587, 1552, 1494, 1475, 1418, 1381, 1344, 1297, 1247, 1171, 1131, 1098, 1048, 930, 894, 745, 701, 559, 472 and 368 cm^{-1}. These bands are associated to the KH tautomer of AR26.

On the contrary, when exciting at 532 nm (Fig. 4b), good SERS spectra of AR26 are obtained, due to the pre-resonant conditions met at this excitation line. The most intense SERS bands are observed at pH $\leq$ 3. This is due to the strong interaction of AR26 with the Ag NST at low pH, due to the protonation of citrate ions as explained above. Thus, Ag substrates can interact with sulfonate molecules, such as AR26. Thus, at acidic conditions well resolved and intense bands are observed at 1601, 1584, 1493, 1476, 1382, 1345, 1299, 1274, 1246, 1226, 1190, 1170, 1135, 1050, 939, 898, 744, 675, 555, 492, 472 and 373 cm^{-1}. As in the previous case, these bands are due to the KH tautomer of the dye. SERS spectra at pH 4 and 5 show similar intensity. However, the addition of different amounts of NaOH to reach basic pH conditions, leads to a strong decrease in the intensity of the SERS bands at pH 7 and to a total absence of bands at pH 10.

The impossibility of obtaining SERS spectra at alkaline pH prevents the detection of the HA tautomer as well, since the appearance of this tautomeric structure requires a strong increase of pH, and the *ortho*- position of the OH group in AR26 leads to the stabilization of the KH tautomer up to pH 11.

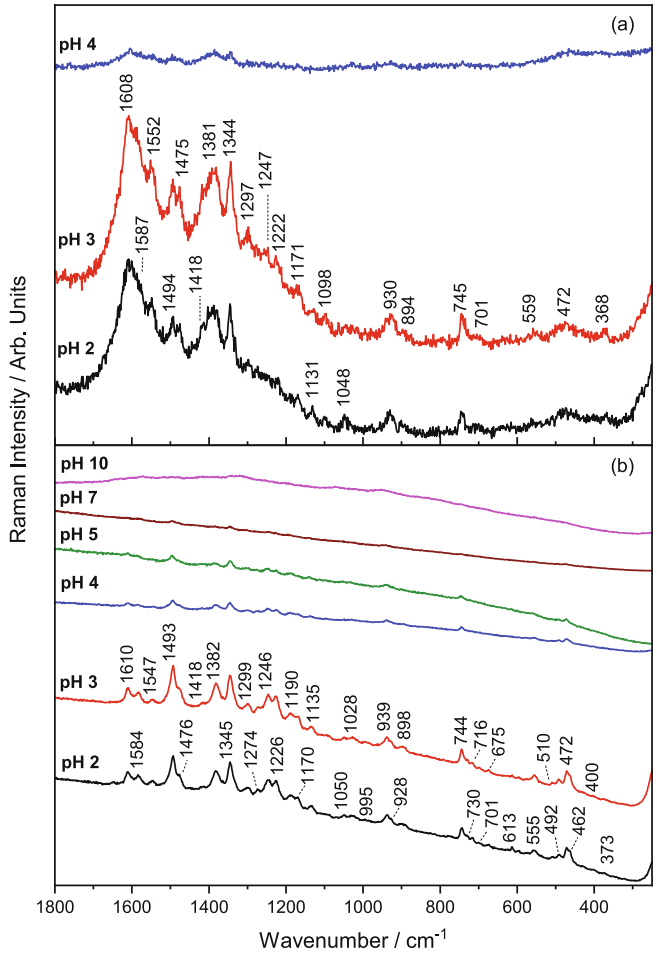

Fig. 4. SERS spectra of 10^{-5} M solutions of AR26 on Ag NST at various pH conditions and excitation at (a) 442 and (b) 532 nm.

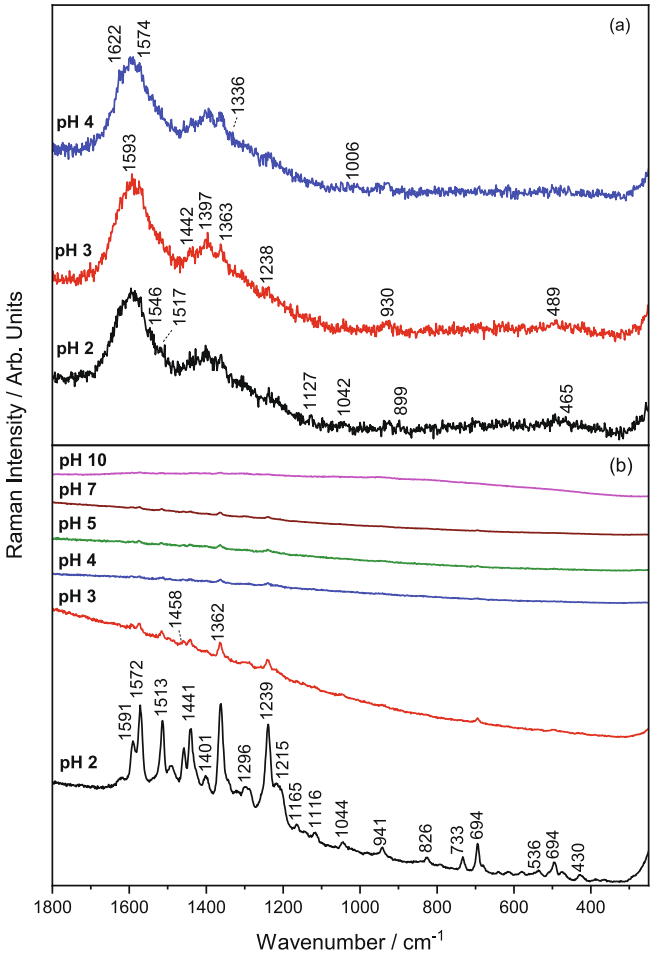

Fig. 5. SERS spectra of 10–5 M solutions of AR18 on Ag NST at various pH conditions and excitation at (a) 442 and (b) 532 nm.

3.3.2. AR18

Fig. 5 shows the SERS spectra of 10^{-5} M aqueous solutions of AR18. The use of the 442 nm laser gives rise to the appearance of the typical pair of bands of amorphous carbon, as occurred in the analysis of AR26. In this case, the burning of the dye is stronger, as very weak bands of the dye are observed at 1622, 1593, 1574, 1546, 1517, 1442, 1397, 1363, 1336, 1127, 1042, 1006, 930, 899, 489 and 465 cm^{-1}. These SERS bands are associated to the KH tautomer, as in the case of AR26. The intensity of the AR18 bands decrease as the pH increases. Thus, no SERS bands are observed at pH $\geq$ 5.

At 532 nm (Fig. 5b), the SERS spectra of AR18 also show bands at 1617, 1591, 1572, 1490, 1441, 1401, 1392, 1296, 1239, 1215, 1165, 1116, 1044, 941, 826, 733, 694, 536, 496, 473 and 430 cm^{-1}. These bands are assigned to the KH tautomer. The intensity of the SERS spectra decreases as the pH goes from 2 to 10. Thus, the best conditions for the detection of AR18 by SERS is the use of the lowest pH, i.e. 2. At pH 10, no bands of the red dye can be observed. As the number of sulfonate groups of AR18 is higher than of AR26 (3 *vs.* 2), the best pH conditions for the analysis of the former are lower (2 *vs.* 3) than for the latter.

3.4. Comparison of the Raman and SERS spectra: adsorption mechanism

Fig. 6a shows the comparison of the Raman and SERS spectra of AR26 at 532 nm. Only a slight difference can be seen between both spectra thus indicating that the interaction with the metal is not affecting so much the dye structure. As the sulfonic group protonation is needed for the approaching of AR26 to the surface, no interaction through these groups with the metal occurs. As the SERS spectra are mainly obtained at low pH, a higher protonation of acidic groups is expected in the citrate ions adsorbed on the surface. Thus, an interaction of the dyes through the establishment of H-bond is suggested. These interactions are strong enough to ensure the necessary approach of the molecule to the surface and the subsequent SERS intensification. Nevertheless, a relative intensification of bands corresponding to the naphtyl groups in the 1200–1300 cm^{-1} interval can be observed. In this case, as the differences between the Raman and SERS spectra are very little, it is difficult to assess the adsoption mechanism of AR26 onto the Ag NST. It only could be guessed that the dye molecule should lie perpendicular to the metallic surface, as no intensity decrease is observed in the aromatic stretching vibrations.

Fig. 6b shows the comparison of the Raman and SERS spectra of AR18 at 532 nm. As in the case of AR26, only slight differences can be seen between both spectra. Therefore, a perpendicular adsorption of the AR18 molecule on the Ag surface could be suggested.

3.5. SERS analysis of a red dyed fiber

An aqueous solution of AR18 was obtained by extraction from a fiber dyed with the red colorant. This sample was analyzed by SERS at acid pH with excitation at 532 nm. Both the original and the

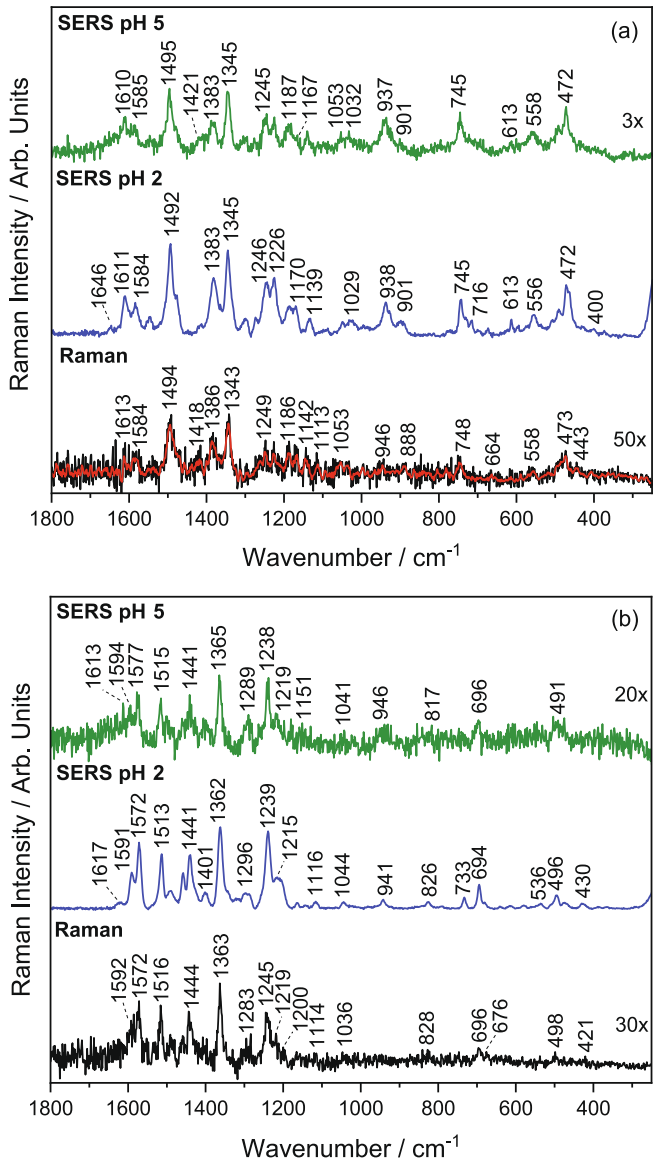

Fig. 6. Raman (10^{-2} M) and SERS (10^{-5} M) spectra at pH 2 and 5 of aqueous solutions of (a) AR26 and (b) AR18 dyes. All spectra were baseline-corrected. A 5 points adjacent-averaging smoothing was applied to the Raman spectrum in (a) (red spectrum). Excitation at 532 nm.

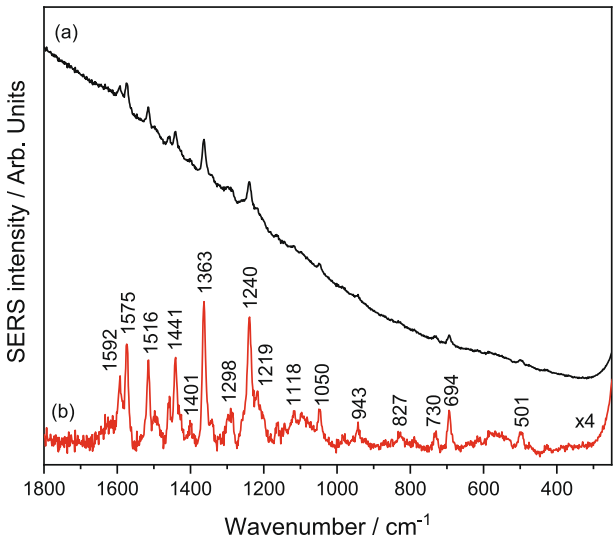

Fig. 7. SERS spectra and pH ~ 2 of an extract of AR18: (a) original and (b) baseline-corrected. Excitation at 532 nm.

baseline-corrected SERS spectra are shown in Fig. 7. The main bands of the spectra are observed at 1592, 1575, 1516, 1457, 1441, 1401, 1363, 1298, 1240, 1219, 1118, 1050, 943, 827, 730, 694 and 501 cm^{-1}. This bands can be undoubtedly assigned to the red dye AR18. Therefore, the use of the proposed experimental conditions is suitable for the SERS analysis of this red dyes.

4. Conclusions

In this work, the monoazo dyes Acid Red 26 and Acid Red 18 were analyzed by UV–Vis, Raman and SERS spectroscopies. These dyes undergo an azo-hydrazone tautomerism. These techniques were applied in order to evaluate the preponderance of one tautomer over the other in different pH conditions. The obtained results were compared to those obtained for Acid Orange 20, another monoazo dye previously studied. The UV–Vis spectra of AR26 and AR18 showed that at pH < 11 and 9, respectively, both dyes were present as the KH tautomer. At higher pH values, HA was prevalent. As both red dyes have the OH in *ortho-* position related to the azo group, a six-membered ring is formed by the intramolecular hydrogen bond OH---N=N. This ring stabilizes the KH form, leading to an increase of the pK_a of the tautomeric equilibrium, compared to that of AO20, which have the OH in *para-*. The Raman spectra of the solid samples and aqueous solutions of AR26 and AR18 at different excitation wavelengths showed bands that correspond to the KH tautomer. Vibrations obtained by DFT calculations of the AR26 and AR18 tautomers were successfully assigned to the experimental Raman bands of KH and HA. The SERS spectra of both dyes at 442 nm show a strong background due to the burning of the sample, which makes difficult to observe the SERS bands of the dye. However, at 532 nm, very strong bands are observed due to a pre-resonance effect of the dyes at this excitation line. The SERS enhancement is greater for both dyes at acid pH, around 2 and 3, and rapidly decreases as the pH increases. At pH 10, no SERS bands are observed for any dye. Thus, only the KH tautomer could be detected by SERS spectroscopy. According to this results, the best experimental conditions for the analysis of both monoazo red dyes in works of art are the use of a pH around 2, and the excitation line of 532 nm. Thus, the obtained SERS spectra will benefit from the interaction of the dye with the Ag nanoparticles and the pre-resonance effect that increases the enhancement. Furthermore, the interaction of dyes with the surface seems to take place through the H-bond formation between the highly protonated citrate ions existing on the NP surface and the sulfonic groups in the dyes. Finally, the optimal experimental conditions were used to analyze an aqueous solution containing AR18 extracted from a fiber dyed with thit colorant. The SERS bands corresponding of the red dye were observed in the spectrum, making possible the identification of AR18, the dye used in the fiber sample.

CRediT authorship contribution statement

Giulia Vannucci: Investigation, Visualization. **Maria Vega Cañamares:** Conceptualization, Formal analysis, Writing - original draft, Writing - review & editing. **Silvia Prati:** Resources, Supervision. **Santiago Sanchez-Cortes:** Resources, Supervision, Funding acquisition, Writing - review & editing.

Declaration of Competing Interest

The authors declare that they have no known competing financial interests or personal relationships that could have appeared to influence the work reported in this paper.

Acknowledgements

This work was supported by Ministerio de Economía, Industria y Competitividad de España (project FIS2017-84318-R) and Comunidad de Madrid/EU (project TOP Heritage).

Appendix A. Supplementary material

Supplementary data to this article can be found online at https://doi.org/10.1016/j.saa.2021.120007.

References

[1] J.C. Barnett, Synthetic organic dyes, 1856–1901: an introductory literature review of their use and related issues in textile conservation, Stud. Conserv. 52 (sup1) (2007) 67–77, https://doi.org/10.1179/sic.2007.52.Supplement-1.67.
[2] M. Snehalatha, C. Ravikumar, I.H. Joe, N. Sekar, V.S. Jayakumar, Spectroscopic analysis and DFT calculations of a food additive carmoisine, Spectrochim. Acta Part A Mol. Biomol. Spectrosc. 72 (2009) 654–662, https://doi.org/10.1016/j.saa.2008.11.017.
[3] A. Bowes, S. Collins, S. Elliott, H. La Tasha, L. Hazlett, E. Méthé, M. Razak, P.Y. Subagiyo, Important Early Synthetic Dyes: Chemistry, Constitution, Date, Properties, Smithsonian Institution, Washington D.C, 1991.
[4] R.W. Horbin, J.A. Kiernan, Conńs Bioloical Stains. A Handbook of Dyes, Stains and Fluorochromes for Use in Biology and Medicine, 10th Ed., BIOS Scientific Publications, Oxford, 2002.
[5] P. Gori, Ponceau 2R staining on semi-thin sections of tissues fixed in glutaraldehyde-osmium tetroxide and embedded in epoxy resins, J. Microsc. 110 (1977) 163–165, https://doi.org/10.1111/j.1365-2818.1977.tb00028.x.
[6] J. Abbey, B. Fields, M. O'Mullane, L.D. Tomaska, Food additives: colorants, in: Y. Motarjemi, G. Moy, E. Todd (Eds.), Encyclopedia of Food Safety, 2, Academic Press, San Diego, CA, 2013, pp. 459–465.
[7] S.A. Centeno, Identification of artistic materials in paintings and drawings by Raman spectroscopy: some challenges and future outlook, J. Raman Spectrosc. 47 (2016) 9–15, https://doi.org/10.1002/jrs.4767.
[8] J.M. Madariaga, Analytical chemistry in the field of cultural heritage, Anal. Methods 7 (2015) 4848–4876, https://doi.org/10.1039/C5AY00072F.
[9] J.R. Lombardi, R.L. Birke, A unified approach to surface-enhanced Raman spectroscopy, J. Phys. Chem. C 112 (2008) 5605–5617, https://doi.org/10.1021/jp800167v.
[10] F. Pozzi, S. Zaleski, F. Casadio, M. Leona, J.R. Lombardi, R.P. Van Duyne, Surface-enhanced raman spectroscopy: using nanoparticles to detect trace amounts of colorants in works of art, in: P. Dillmann, L. Bellot-Gurlet, I. Nenner (Eds.), Nanoscience and Cultural Heritage, Atlantis Press, Paris, 2016. https://doi.org/10.2991/978-94-6239-198-7_6.
[11] A. Cesaratto, S.A. Centeno, J.R. Lombardi, N. Shibayama, M. Leona, A complete Raman study of common acid red dyes: application to the identification of artistic materials in polychrome prints, J. Raman Spectrosc. 48 (2017) 601–609, https://doi.org/10.1002/jrs.5082.
[12] G. Vannucci, M.V. Cañamares, S. Prati, S. Sanchez-Cortes, Study of the azo-hydrazone tautomerism of Acid Orange 20 by spectroscopic techniques: UV-visible, Raman and SERS, J. Raman Spectrosc. 51 (2020) 1295–1304, https://doi.org/10.1002/jrs.5906.
[13] P. Ball, C.H. Nicholls, Azo-Hydrazone tautomerism compounds – a review, Dyes Pigm. 3 (1982) 5–26, https://doi.org/10.1016/0143-7208(82)80010-7.
[14] M.A. Rauf, F. Hisaindee, N. Saleh, Spectroscopic studies of keto-enol tautomeric equilibrium of azo dyes, RSC Adv. 5 (2015) 18097–18110, https://doi.org/10.1039/C4RA16184J.
[15] A. Garcia-Leis, J.V. Garcia-Ramos, S. Sanchez-Cortes, Silver nanostars with high SERS performance, J. Phys. Chem. C 117 (2013) 7791–7795, https://doi.org/10.1021/jp401737y.
[16] M.J. Frisch, G.W. Trucks, H.B. Schlegel, G.E. Scuseria, M.A. Robb, J.R. Cheeseman, G. Scalmani, V. Barone, G.A. Petersson, H. Nakatsuji, X. Li, M. Caricato, A. Marenich, J. Bloino, B.G. Janesko, R. Gomperts, B. Mennucci, H.P. Hratchian, J.V. Ortiz, A.F. Izmaylov, J.L. Sonnenberg, D. Williams-Young, F. Ding, F. Lipparini, F. Egidi, J. Goings, B. Peng, A. Petrone, T. Henderson, D. Ranasinghe, V.G. Zakrzewski, J. Gao, N. Rega, G. Zheng, W. Liang, M. Hada, M. Ehara, K. Toyota, R. Fukuda, J. Hasegawa, M. Ishida, T. Nakajima, Y. Honda, O. Kitao, H. Nakai, T. Vreven, K. Throssell, J.A. Montgomery, Jr., J.E. Peralta, F. Ogliaro, M. Bearpark, J.J. Heyd, E. Brothers, K.N. Kudin, V.N. Staroverov, T. Keith, R. Kobayashi, J. Normand, K. Raghavachari, A. Rendell, J.C. Burant, S.S. Iyengar, J. Tomasi, M. Cossi, J.M. Millam, M. Klene, C. Adamo, R. Cammi, J.W. Ochterski, R. L. Martin, K. Morokuma, O. Farkas, J.B. Foresman, D.J. Fox, Gaussian 09, Revision A.02, Gaussian, Inc., Wallingford CT, 2016.
[17] P. Scott, L. Radom, Harmonic vibrational frequencies: an evaluation of Hartree−Fock, Møller−Plesset, quadratic configuration interaction, density functional theory, and semiempirical scale factors, J. Phys. Chem. 100 (1996) 16502–16513, https://doi.org/10.1021/jp960976r.
[18] X.-C. Chen, T. Tao, Y.-G. Wang, Y.-X. Peng, W. Huang, H.-F. Qian, Azo-hydrazone tautomerism observed from UV-vis spectra by pH control and metal-ion complexation for two heterocyclic disperse yellow dyes, Dalton Trans. 36 (2012) 11107–11115, https://doi.org/10.1039/C2DT31102J.
[19] M. Pérez-Urquiza, J.L. Beltrán, Determination of the dissociation constants of sulfonated azo dyes by capillary zone electrophoresis and spectrophotometry methods, J. Chromatogr. A 917 (2001) 331–336, https://doi.org/10.1016/S0021-9673(01)00707-5.
[20] P. Sierra-Rosales, C. Berríos, S. Miranda-Rojas, J.A. Squella, Experimental and theoretical insights into the electrooxidation pathway of azo-colorants on glassy carbon electrode, Electrochim. Acta 290 (2018) 556–567, https://doi.org/10.1016/j.electacta.2018.09.090.
[21] K. Bevziuk, A. Chebotarev, D. Snigur, Y. Bazel, M. Fizer, V. Sidey, Spectrophotometric and theoretical studies of the protonation of Allura Red AC and Ponceau 4R, J. Mol. Struct. 1144 (2017) 216–224, https://doi.org/10.1016/j.molstruc.2017.05.001.
[22] E. Hofer, H. Huffmann, Tautomerie von 4-hydroxy-azobenzolen, Tetraedron Lett. 35 (1971) 3241–3244, https://doi.org/10.1016/S0040-4039(01)97145-X.
[23] M.R. Almeida, R. Stephani, H.F. Dos Santos, L.F.C. de Oliveira, Spectroscopic and theoretical study of the "Azo"-Dye E124 in condensate phase: evidence of a dominant hydrazo form, J. Phys. Chem. A 114 (2010) 526–534, https://doi.org/10.1021/jp907473d.